WILEY

Near-source ground motion in the M7.8 Gaziantep (Turkey) earthquake

Georgios Baltzopoulos[1] | Roberto Baraschino[2] | Eugenio Chioccarelli[3] | Pasquale Cito[1] | Antonio Vitale[1] | Iunio Iervolino[1,4]

[1]Università degli Studi di Napoli Federico II, Naples, Italy

[2]Studio SPERI, Naples, Italy

[3]Università degli Studi Mediterranea di Reggio Calabria, Reggio Calabria, Italy

[4]IUSS – Scuola Superiore Universitaria di Pavia, Pavia, Italy

Correspondence
Iunio Iervolino, Dipartimento di Strutture per l'Ingegneria e l'Architettura, Università degli Studi di Napoli Federico II, via Claudio 21, 80125, Naples, Italy.
Email: iunio.iervolino@unina.it

I, Iunio Iervolino, confirms that all the authors are aware of the submission to EESD, and consent to it.

Abstract
On the night of February 6, 2023, a major earthquake struck Turkey and nearby Syria, whose moment magnitude (M) was estimated at 7.8 (or 7.7, depending on the data source). It started what can be considered a seismic sequence with thousands of recorded earthquakes with magnitude larger than two, including another M6.7 event (or 6.6) occurring shortly after, and one M7.5 (or 7.6) a day and a half later. The area in the south-eastern part of Turkey hit by the sequence is considered, according to probabilistic models, one of the most hazardous in the wider region. This technical note aims at a preliminary illustration of some features of the shaking, deemed of earthquake engineering relevance. To this aim, it preliminarily analyzes the evolution of the sequence so far and the related ground motion intensity, as estimated from ShakeMap envelopes, then focuses on the largest magnitude event, for which a preliminary model of the source is available, while a supplementary report is provided for the other two events. Based on data available at the time of writing, it is found that the development of the sequence and the recorded ground motions are generally in agreement with available models, although some locations may have experienced peak ground accelerations larger than 1.0 g, and near-source effects, determining pulse-like ground motions, apparently occurred.

KEYWORDS
aftershock sequence, earthquake data, pulse-like ground motions, response spectra

1 | INTRODUCTION

On February 6, 2023, at 1.17 UTC (local time 4:17 AM, UTC+3), a major earthquake occurred with epicenter (long. 37.01°E, lat. 37.23°N) close to the city of *Gaziantep*, affecting a large region in Turkey and nearby Syria. Its moment magnitude (M) was estimated at M7.7 according to *Afet ve Acil Durum Yönetimi Başkanlığı* or AFAD (see Data and resources). The most recent available model of the rupture at the time of writing, provided by the US Geological Survey (USGS; see Data and resources), attributes to it magnitude equal to 7.8, which is also adopted in the present paper and other sources (to follow).

NOVELTY

1. Analysis of the Turkey-Syria sequence so far.
2. Comparison of spectra with ground motion prediction equation (GMPE).
3. Analysis for pulse-like ground motions.
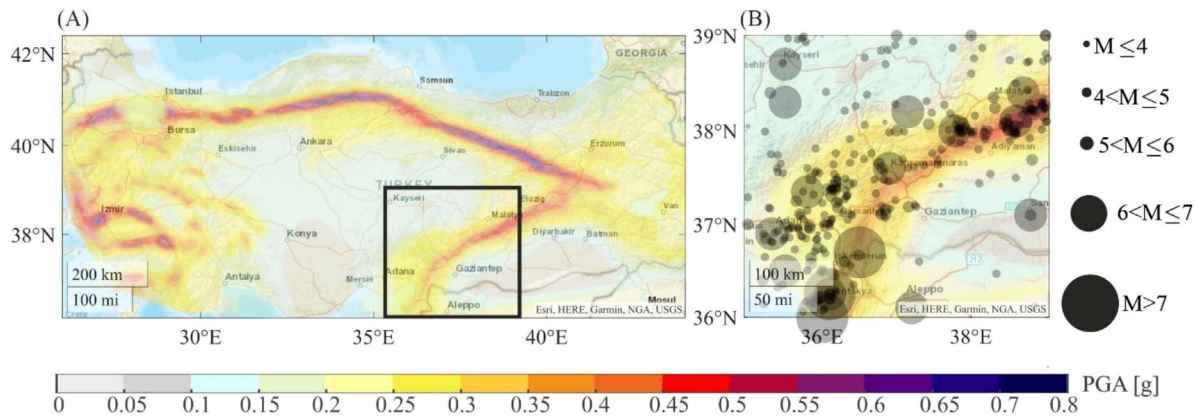4. Larger analyses for the three main events provided in a supplementary report.

FIGURE 1   (A) ESHM20 hazard map of Turkey; (B) earthquake catalog for the zone of the sequence.

According to the USGS model, the fault length is several hundreds of kilometers with the rupture consisting of three segments and is bi-lateral. The M7.8 event started what can be considered a seismic sequence of about $7 \cdot 10^3$ (at the time of writing) recorded earthquakes of magnitude larger than M2.0, including a M7.5 event, one M6.7, and one M6.3. The fault mechanism for the M7.8 and M7.5 events is reported by available rupture models to be strike-slip and the same is expected for the other two mentioned M6.0+ events.[1] The hypocentral depth of the M7.8, M7.5, and M6.7 events is reported between seven and ten kilometers, while for the M6.3 event it is set around twenty kilometers.

The area hit by the sequence, which extends over several hundreds of square kilometers, is in the south-eastern part of Turkey, close to Syria, part of which was also affected by the shaking. Together with the North-Anatolian fault system and the western part of the country, the affected area is the most seismically hazardous according to a recent probabilistic seismic hazard assessment for Europe, that is, ESHM20.[2] This can be seen in Figure 1A, where the long-term seismic hazard in terms of peak ground acceleration (PGA) on rock with exceedance return period (T_r) equal to 476 years is mapped for about $8 \cdot 10^3$ sites within a grid (with 0.1° node spacing) covering the whole country, together with the frame of the zone affected by the sequence. As a complement, Figure 1B shows an earthquake catalog for the region.[3]

This technical note aims at a timely, yet preliminary, illustration to the earthquake engineering community of the main features of the sequence as recorded so far, and related ground shaking. More specifically, the evolution of the sequence in terms of magnitude, time, and location, is illustrated in the next section and is compared to what is expected by a classic model. Also, the ground motion intensities, in terms of PGA, estimated by ShakeMap (v4.0)[4] for all the events of the sequence with magnitude equal to or larger than M6.0, and made available by the USGS (Data and resources), are compared to the ESHM20 hazard map to estimate the portion of the country that possibly experienced exceedance of the hazard map's PGA values. Then, the remainder of the document focuses on the (so far) largest magnitude event of the sequence. However, the interested reader can find more information, also on the other two large-magnitude earthquakes, in a dedicated report that complements this short article.[5] Regarding the chosen event, Section 3 shows the spectra recorded in the vicinity of the identified rupture and compares them with what is expected by a ground motion prediction equation (GMPE) calibrated for the region.[6] One of the records exhibiting the most intense spectra is analyzed in greater detail. Finally, Section 4 investigates for possible records of pulse-like ground motion. Some concluding remarks summarize the main preliminary findings.
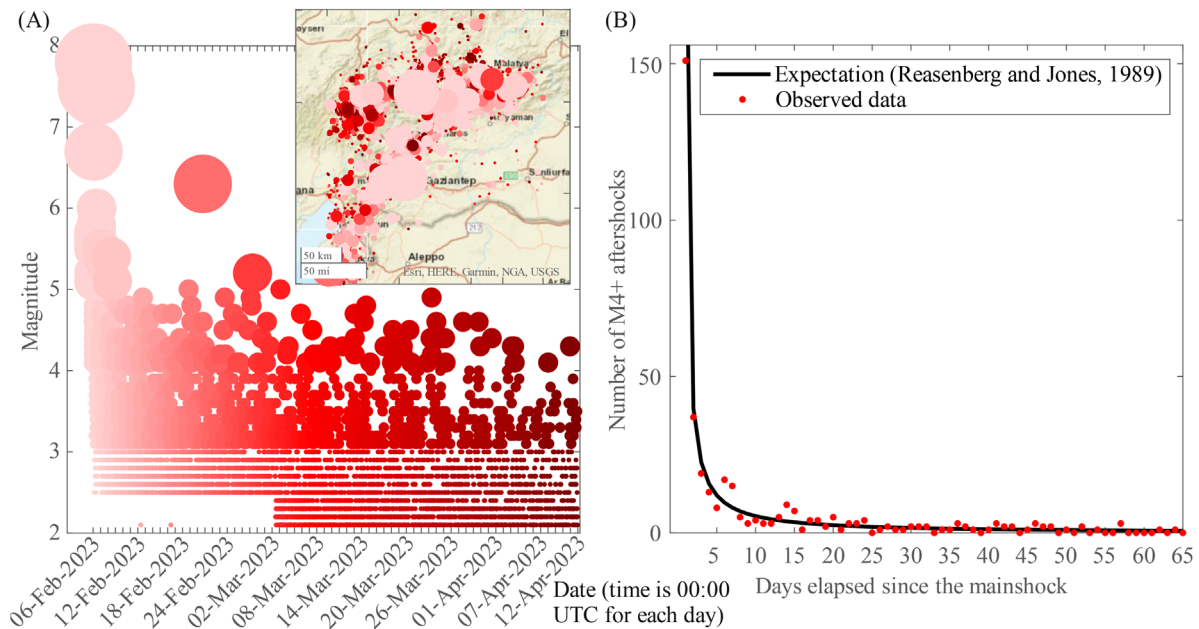
FIGURE 2 (A) Time-space evolution of the sequence up to April 11, 2023; (B) daily recorded earthquakes M4+ and corresponding expected values according to the modified Omori law with parameters for California.

2 | THE SEQUENCE

Earthquakes typically occur as clusters (sometimes also indicated as seismic sequences), that is, they are concentrated in time and space.[7] Following a typical classification, the largest magnitude event in the cluster is recognized herein as the *mainshock*, and all the earthquakes recorded before and after it, in some time-space window, are identified as foreshocks and aftershocks, respectively. However, such mainshock/aftershock discrimination may not be univocal; for example, the second largest magnitude M7.5 event, recorded a few hours after M7.8 and relatively close to it (to follow), is assumed as an aftershock of M7.8 by Schmitt et al.,[8] whereas Stein et al.[9] identify both M7.8 and M7.5 events as mainshocks.

February 6, 2023, M7.8 is the first event of a sequence with about $6.9 \cdot 10^3$ earthquakes above magnitude two, that had been recorded up to (and including) April 11, in an area $9 \cdot 10^4$ km^2 wide, extending from longitude 36°E to 39°E and from latitude 36°N to 39°N, amounting to more than $1 \cdot 10^2$ events per day, on average. This area includes the Turkish provinces damaged by the sequence, such as Osmaniye and Şanlıurfa, from West to East, as well as Hatay, Gaziantep, and Malatya, including Kahramanmaraş, from South to North. The evolution of the sequence in terms of magnitude versus time, for the events that had been recorded from February 6, 00:00 (UTC) until the end of April 11 and with epicenters falling within the considered area, is shown in Figure 2A, together with the location of the events. Data for this figure were derived from the dedicated *European Plate Observing System* (EPOS) services (see Data and resources). However, the figure reveals that some completeness issues had likely occurred during the first month of the sequence (up until March 2 to be precise), as there are not any data available for earthquakes of magnitude below M2.5 for that period.

In Figure 2A, where the size and color nuance of the markers vary with earthquake magnitude and time of occurrence, respectively, the largest magnitude event of M7.8 is the first one. In fact, in this particular case, no foreshocks are attributed to the sequence under examination, at least according to available data. About 10 min after the mainshock, and at less than 25 km away from its epicenter, a M6.7 event occurred. The data reveal that, during the first hour after the mainshock, eight earthquakes with magnitude equal to, or larger than, M5.0 were recorded. (For comparison, the same number of M5.0+ events occurred over five months during the long-lasting 2016−2017 central Italy seismic sequence.)[10]

In this (Kahramanmaras) sequence, about $1.6 \cdot 10^2$ events were recorded up to 10:24 (UTC) on February 6, most of which with magnitude below five. Then, the second strongest event, M7.5, occurred about 100 km north of the main-shock, followed by about twenty earthquakes in the next 90 min, half of which with magnitude larger than M4.5. Up to that point, according to EPOS data, about $1.8 \cdot 10^2$ earthquakes had been recorded within 12 h, two of which with magnitude larger than M7.0. Starting from 12:00 (UTC) of February 6 and until 14:20 (UTC) of February 8, the magnitude of detected events did not exceed M6.0, while $1.6 \cdot 10^1$ earthquakes were recorded with magnitude equal to larger
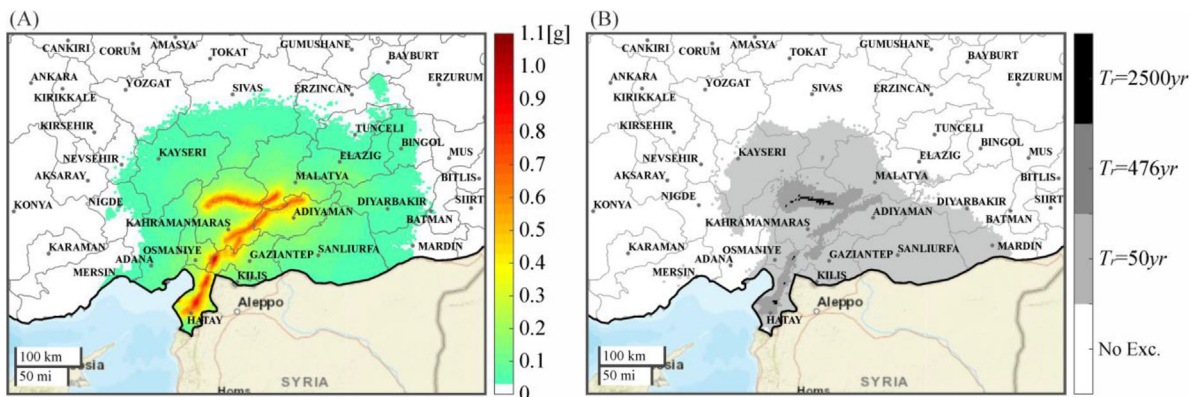
FIGURE 3 (A) Shakemap envelope for M6.0+ events of the sequence; (B) area subjected to at least one exceedance of the PGA from the ESHM20 hazard assessment due to the M6.0+ events.

than M5.0. From that point on, the magnitude of the events recorded in the next 12 days (that is, from February 8 to 20) did not exceed five, with most of them being below M4.0 (about $1.7 \cdot 10^3$ out of a total of $1.8 \cdot 10^3$). After $2.6 \cdot 10^3$ earthquakes had been recorded since the beginning of the sequence, Turkey was hit by another M6.3 earthquake on February 20, at 17:04 (UTC), with epicenter found in proximity to the Turkey-Syria border region. About $1.0 \cdot 10^3$ earthquakes, two of which with magnitude between M5.0 and M5.2, were recorded in the two following weeks. From March 3 to April 11, the magnitude of the $3.3 \cdot 10^3$ recorded events remained below M5.0, and a significant fraction of them was even below M3.0.

Having identified the M7.8 event as the mainshock and those recorded after it, in the area mapped in Figure 2A, as aftershocks, it may be interesting to investigate whether the temporal trend of the sequence is compatible with what is predicted by the *modified Omori law*,[11] which allows one modeling the expected number of aftershocks as a function of the time elapsed from the mainshock. Such a comparison is displayed in Figure 2B. The curve gives the expected number of aftershocks per day, after the M7.8 mainshock, according to the Omori law, with parameters calibrated for California (US),[12] while the red dots represent the daily numbers of M4+ events recorded up to April 11 (included). The figure shows that the daily expected values from the modified Omori law, despite its parameters being calibrated for California, are somewhat in agreement with the observations of earthquakes with magnitude equal to, or larger, than four.

As an additional consideration, the portion of Turkey that has been possibly subjected to (at least one) exceedance of the $T_r = 476$ yr PGA value from the ESHM20 hazard map, is quantified considering the PGA ShakeMap for the six earthquakes of the sequence with magnitude equal to or larger than M6.0 (whose epicenters are shown in Figure 2A). The PGA envelope of all six events, computed at the sites of the same grid used to represent the hazard map, is shown in Figure 3A.[10] The largest (estimated) PGAs are found in proximity to the areas hit by the M6.0 and M6.0+ events, with a value as high as about 1.1 g mapped in the Gaziantep province, at about 35 km from the mainshock epicenter.

The comparison of the ShakeMap envelope with the PGA values from the ESHM20 hazard map for $T_r = 476$ yr (the one in Figure 1A) allows identifying the sites (map grid cells) where exceedance has possibly occurred in at least one of the M6.0 and M6.0+ events. These are contained within the dark gray area (i.e., the exceedance area) mapped in Figure 3B. The panel also shows the exceedance areas for $T_r = 50$ yr and $T_r = 2500$ yr, which are colored in light gray and black, respectively (hazard maps for these return periods are not shown for the sake of brevity), while white areas are those where no exceedance was observed for any of the considered return periods or where no ground motion data are available from ShakeMap. In quantifying the exceedance area, hazard thresholds were adjusted for the site soil conditions, as accounted for by ShakeMap, via soil-specific coefficients provided by the GMPE adopted by ESHM20, that is, the model of Kotha et al.[13] Also, because that GMPE considers the rotated median RotD50 of the two horizontal components of ground motion, hazard thresholds were adjusted for the largest component, which is the metric used by ShakeMap, according to Beyer and Bommer.[14,15]

For each return period, the fraction of Turkey that possibly experienced at least one exceedance, according to ShakeMap, was calculated. Table 1 shows that the fraction of the country estimated to have been exposed to exceedance is equal to 12.3%, 1.4%, and 0.1% in the case of $T_r = 50$ yr, $T_r = 476$ yr, and $T_r = 2500$ yr, respectively. The table also gives the extent of the exceedance area, which decreases by one order of magnitude when looking at the return periods considered here in ascending order. Considering the M7.8 event alone, the fraction of Turkey possibly subjected to

TABLE 1 Fraction of Turkey possibly exposed to exceedance of the PGA from the ESHM20 hazard map due to the M6.0+ events of the sequence.

| Exceedance area	$T_r = 50$ yr	$T_r = 476$ yr	$T_r = 2500$ yr
%	12.3	1.4	0.1
km^2	96'334	11'264	534

exceedance of the $T_r = 50$ yr PGA is estimated equal to 9.7%. In the case of $T_r = 476$ yr, the estimated exceedance area is about 0.6%.

3 | RESPONSE SPECTRA AND GROUND MOTION PREDICTION

AFAD provided raw and corrected accelerometric data from 379 stations that recorded ground motions during the M7.8 event (last accessed April 7, 2023, see Data and resources). Examination of the raw acceleration waveforms led to the conclusion that 326 records were of sufficient quality to be used for further elaborations, that is, they were devoid of inexplicable or atypical trends in the acceleration time-history, such as apparent abrupt interruptions of the recording, inconsistent with those of nearby stations. All signals were sampled at a rate of 100 Hz and corrected by AFAD implementing a consolidated processing procedure.[16] Because at least one model for the finite fault of the mainshock has
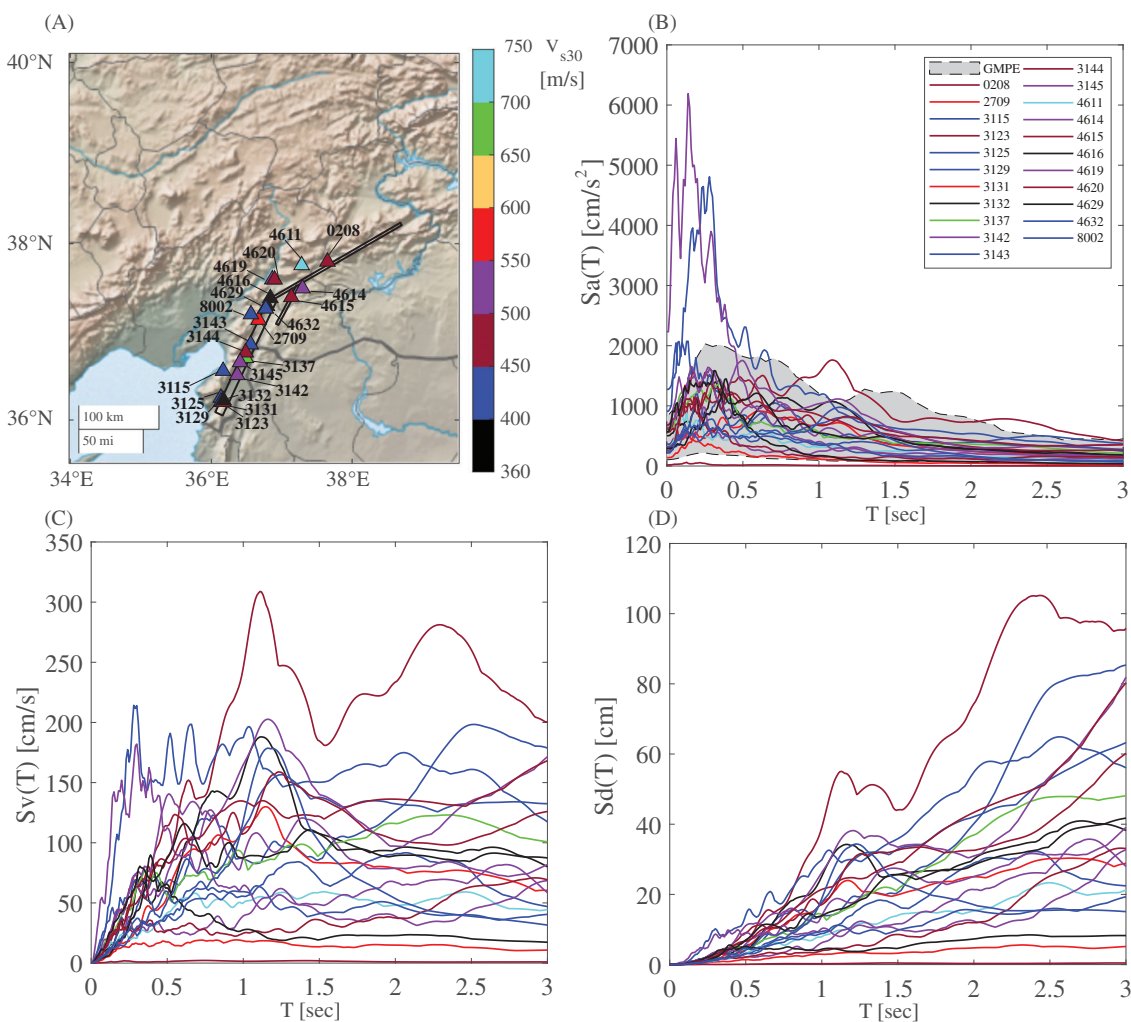
FIGURE 4 (A) Stations within 20 km in terms of R_{jb}; (B) acceleration response spectra for the stiff-soil stations compared with what expected by a GMPE; (C) and (D) velocity and displacement response spectra for the same stiff-soil stations, respectively.
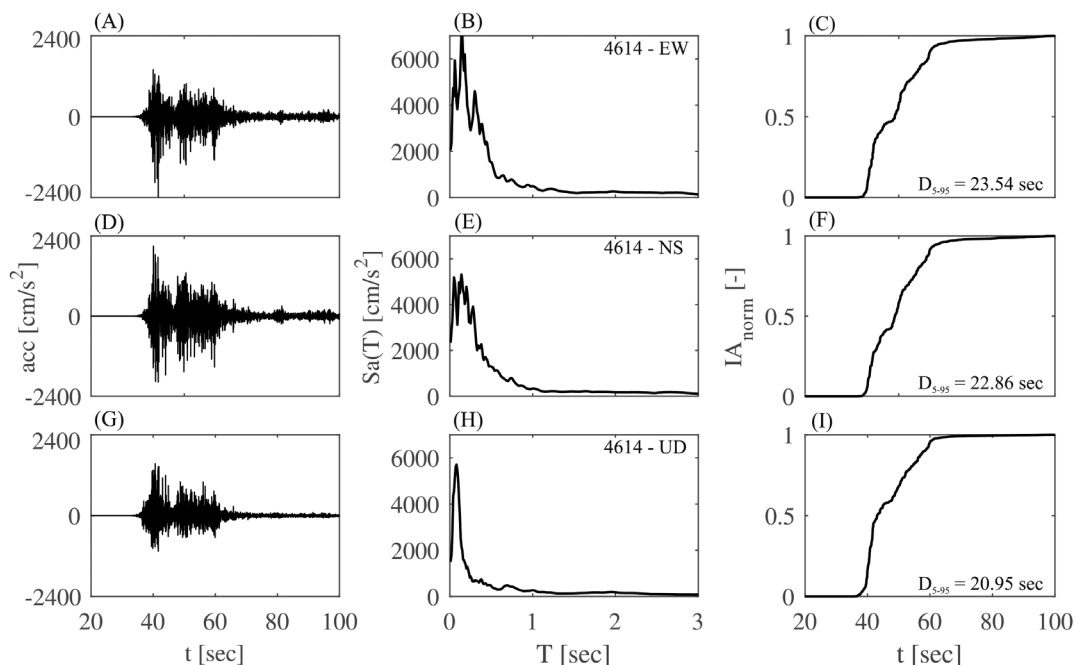
FIGURE 5 (A,D,G) Waveforms of recorded at station 4614; (B,E,H) corresponding pseudo-acceleration response spectra; (C,F,I) corresponding Husid plots.

been made available by USGS, it is possible to identify the stations among these remaining 326 that are closest to the source. More specifically, the stations with Joyner and Boore[17] distance $R_{jb} \leq 20$ km are 244. Among them, the shear-wave velocity in the upper 30 m, or V_{s30}, is available for eighty-eight stations: sixteen stations have $V_{s30} > 750 m/s$, fifty have $V_{s30} < 360 m/s$ and twenty-two stations have $360 \, m/s \leq V_{s30} \leq 750 m/s$. The records from the last group have been compared with expectations of the ground motion model of Akkar et al., cited earlier (considering the corrected parameters),[6,18] which uses R_{jb} as distance metric and distinguishes soil amplification for each of the three V_{s30} ranges given previously.

For each considered recording station, whose location is reported in Figure 4A, the acceleration response spectra of the two horizontal components were combined to compute the geometric mean of each spectral pseudo-acceleration ordinate, $Sa(T)$, that is the ground motion intensity measure considered by the GMPE. The resulting spectra are reported in Figure 4B (the color of each curve is representative of the V_{s30} value; see Figure 4A). Figure 4B also shows the bounds of the exponential of the logarithmic mean from the GMPE at each vibration period, plus and minus one logarithmic standard deviation from the GMPE; the upper bound is computed using $R_{jb} = 0$, whereas the lower bound refers to $R_{jb} = 20$ km. This is to account for all the R_{jb} distances that characterize the selected stations. The area between these two bounds is shaded in gray.

It should be noted that the upper bound of the magnitude range of the GMPE is 7.6 and that this comparison does not include estimates of inter-event terms of the residual for this particular event at all vibration periods, that is, the gray area in the figures considers the total (one-sigma) variability of the GMPE and the median is uncorrected with respect to the event-specific bias. It can be observed that several records featured accelerations larger than 1.0 g at vibration periods of structural interest, that is between 0.5 s and 1.5 s, so that accelerations for the structures close to the recording sites could have been possibly challenging also for constructions following modern seismic design criteria. Nevertheless, the majority of the spectra close to the rupture are generally compatible with what is expected by the GMPE for an event of this magnitude. Notably, the higher-frequency portions of the spectra from stations 4614 and 3129 rise above the one standard deviation line of the GMPE, especially up to a period of 0.5 s. However, it is well-documented that spectral ordinates that supersede GMPE average predictions the most, often correspond to ground motions recorded in proximity to the fault.[19,20] In the medium- and high-period range, the highest velocity and displacement spectra are both from station 3123 and correspond to about 300 cm/s and 100 cm, respectively. That station's record was also identified to exhibit pulse-like features, possibly due to directivity (to follow).

The record from station 4614 features PGA values in excess of 2 g on both horizontal components and could be worthwhile examining in greater detail. To this end, Figure 5 shows the recorded acceleration waveforms, the response

spectra in terms of pseudo-acceleration and the Husid plots,[21] where the significant duration[22] D_{5-95} is also reported. The variations in gradient of the Husid plots between 35 and 65 s could be possibly attributed to the different rates of energy release in sub-events comprising the M7.8 earthquake.

Figure 4C,D shows the corresponding geometric mean of 5% damped spectral pseudo-velocity, $Sv(T)$, and displacement, $Sd(T)$, respectively. More information such as that displayed in Figure 5, for other recordings of the mainshock, as well as for the other main events of the sequence so far can be found in the supplementary report.[5] These complementary analyses show that accelerations, which can be considered significant to the response of structures, may have occurred multiple times within the sequence.

4 | PULSE-LIKE GROUND MOTIONS

This section covers a preliminary analysis of near-source ground motion waveforms from the mainshock, which is investigated for potential pulse-like features (a similar analysis was also conducted for other events in the sequence, although it can be anticipated here that the most of pulse-like ground motions were found in the mainshock).[5] Pulse-like ground motions are of earthquake engineering interest, as they exhibit peculiar spectral shape, characterized by narrowband amplification for both elastic and inelastic spectra and are known for imposing more severe inelastic demand on certain structures than non-impulsive accelerograms, at least on average.[23–25]

The most notorious causes of impulsive ground motion waveforms are certain so-called near-source effects, such as *forward directivity* and *fling-step*. The former refers to sites that are aligned with the direction of rupture propagation along the fault and may thus experience the near-simultaneous arrival of shear waves emitted from different points on the rupture. This so-called forward directivity effect is conspicuously manifest in the ground velocity time-history, where constructive wave interference can cause notable double-side pulses.[26] The latter has to do with permanent ground displacement as a result of the rupture.[27] At this preliminary stage, the analysis is limited to a characterization of certain near-source records as pulse-like based on the features of the ground motion records alone, without circumspect consideration of the physical rupture process in relation to each recording site's location. In this sense, directivity can be considered as one of many possible causes of the impulsive features detected in the investigated records.

Seventy records were examined from the earthquake under consideration. These were initially selected to include the highest available recorded PGA values, on the premise of implied vicinity to the fault, which turned out to be the case, at least based on the assumed rupture geometry that puts these stations within R_{jb} of 20 km or less. Velocity time-histories were obtained via integration of the accelerometric series for both horizontal components of motion, and the resulting vector was rotated over 180° at a step of 1°. For each orientation, a consolidated wavelet-based algorithm was applied to extract candidate pulse waveforms from the velocity time series[28] and to assign a pulse indicator (*PI*) score to each one. This score takes values from 0 to 1 and reflects the degree to which the candidate pulse accounts for the energy content and spectral shape of the entire record. Ground motions were preliminarily characterized as pulse-like if they exhibited a consistently high score of *PI* > 0.90 over an arc of more than 60°, and also exhibited a satisfactory match of the pseudo-velocity spectra of the ground motion and the candidate pulse wavelet, around the pulse period T_P.[29] In this context, pulse period is defined as the pseudo-period of the highest-energy constituent *Daubechies wavelet* of the candidate pulse. This procedure led to the characterization of twenty-one records as pulse-like for the mainshock. Some of the most characteristic velocity time-histories of these pulse-like records, rotated at the orientation of the maximum *PI* score, are shown in Figure 6 below, together with the location of the corresponding stations and the surface projection of the rupture according to the USGS model. That model corresponds to strike-slip faulting with the largest segment at a strike angle of 52° and dipping at 80°. The figure includes arrows next to each station name, indicating the orientation where the largest *PI* score was registered.

From the figure, it can be seen that these sites are generally aligned with the presumed rupture propagation along the strike of each segment, and some also with up-dip propagation, thus apparently satisfying the theoretical premise and empirical expectation for rupture directivity.[30] The sites are also congregated into several groups of higher relative vicinity to one-another: for instance, the NAR and 4615 stations are only about 1.8 km apart, so it is unsurprising that pulses of similar duration were registered in both. The grouping of stations near the southernmost edge of the rupture plane model exhibit pulses that are more clearly manifest toward a fault-parallel orientation, with periods in the 1.8–3.4 s interval.

To assess the significance of these pulses with respect to the seismic actions exerted by each of these ground motions, Figure 7 shows the pseudo-velocity spectra of selected identified pulse-like ground motions from the previous figure, compared with the spectra of the extracted pulse alone.
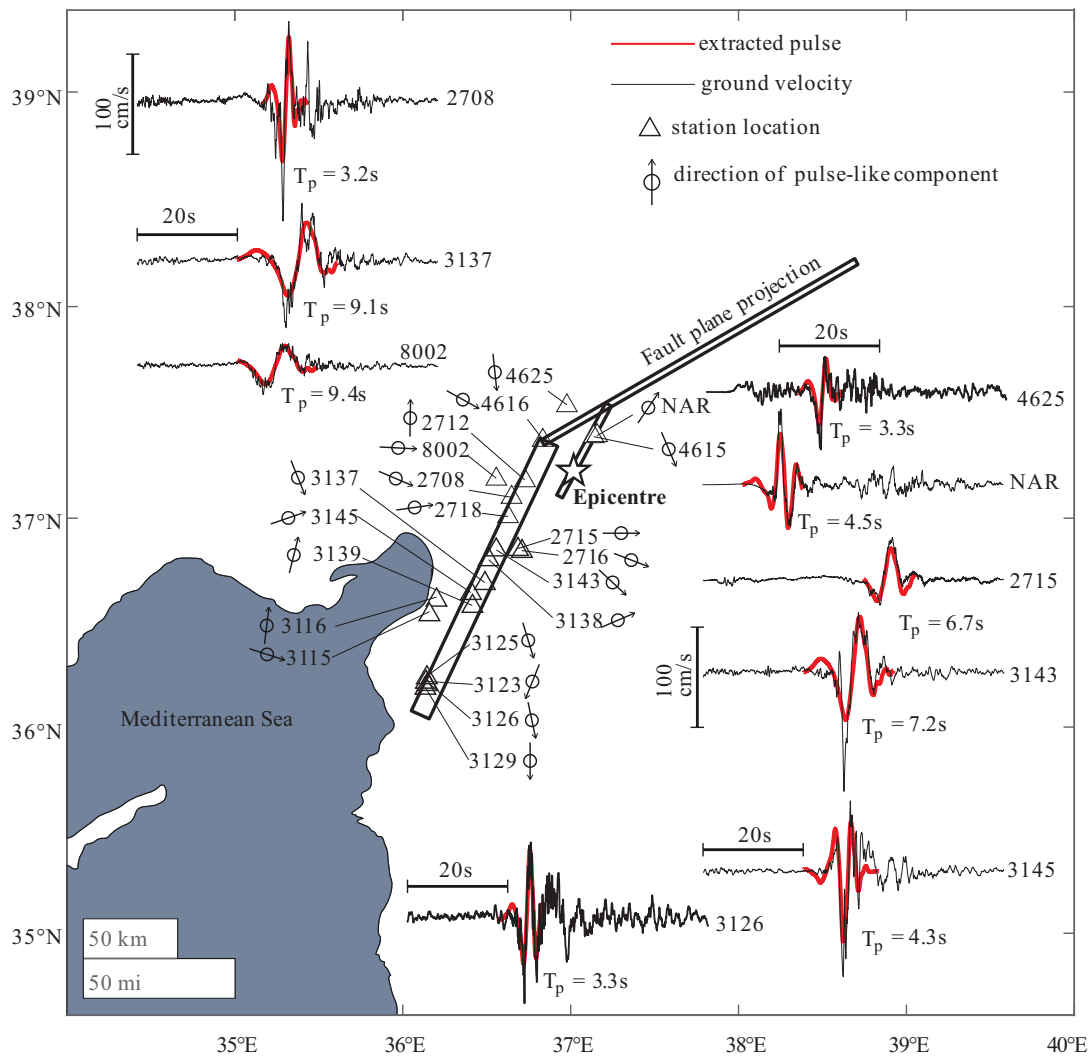
FIGURE 6 Map of the alleged rupture of the M7.8 earthquake and some of the identified velocity pulses.
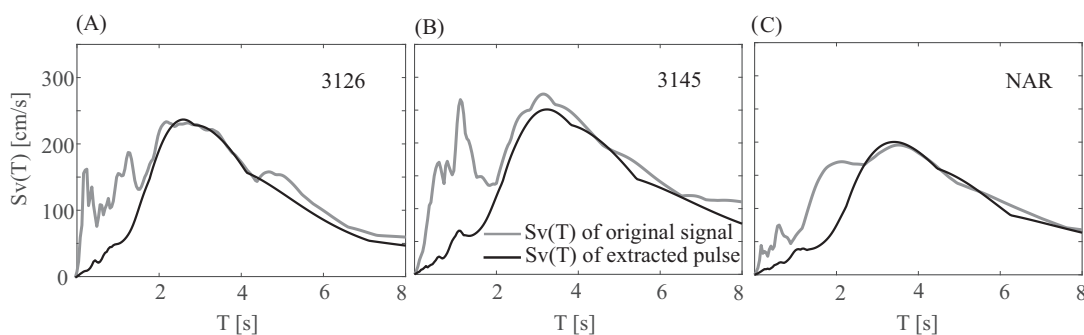

FIGURE 7 Selected pseudo-velocity spectra and spectra of the extracted pulses for three stations.

5 | FINAL REMARKS

On February 6, 2023, at 1.17 UTC, a M7.8 event hit Turkey, then all earthquakes that were recorded during the following two months, with epicenters contained within a $9 \cdot 10^4$ km² wide area enclosing the most damaged Turkish provinces, were identified as aftershocks of a sequence triggered by the M7.8 event, that was classified as the mainshock. The strongest events occurred in the first 12 h, with data showing two M7.0+ events occurring within 100 km from each other. The M7.8

mainshock has been preliminarily analyzed herein. A ShakeMap PGA envelope of the six highest-magnitude events in the sequence, all M6.0+, showed that the 476 years return period PGA from the ESHM20 hazard map was exceeded over an area corresponding to 1.4% of Turkey; for 50 and 2500 years return period PGAs this exceedance area is one order of magnitude higher or lower, respectively.

Spectral accelerations for the mainshock, recorded closest to the source on stiff soil, are generally in agreement with what is expected from the selected (yet extrapolated) GMPE. A couple of records show PGAs larger than 1.0 g and spectral accelerations of several units of g in a period range of structural engineering interest, exceeding the mean plus one-sigma values of the GMPE. An analysis complementing this technical note also highlights that similar accelerations may have occurred multiple times within the sequence due to the other large-magnitude earthquakes observed so far, at unless these records will be revised in the future.

Investigation for pulse-like effects identified near-source pulses, with pulse periods somewhat large, as expected for large magnitude events. Nevertheless, the attribution to these pulses to rupture phenomena (e.g., forward directivity) needs further investigation.

6 | DATA AND RESOURCES

Fatality AFAD data: (last acc. 14/02/2023 10:00 UTC). AFAD ground motion records: https://tadas.afad.gov.tr/list-waveform (last acc. 07/04/2023 12:15 UTC). EPOS earthquake data: https://seismicportal.eu/ (last acc. 12/04/2023 12:00 UTC). ShakeMap data used in this study were obtained from https://earthquake.usgs.gov/earthquakes/map/ (last acc. 20/04/2023 20:30 UTC). Probabilistic seismic hazard data were obtained from http://hazard.efehr.org/en/hazard-data-access/hazard-maps/. ESM Ground motion records: https://esm-db.eu/ (last acc. 18/04/2023). Preliminary finite fault geometry from the USGS, (last acc. 22/04/2023 00:40:00 UTC): https://earthquake.usgs.gov/earthquakes/eventpage/us6000jllz/finite-fault. Additional analyses and data about this and the other main events of the sequence are provided in a supplementary report. [5] It should be highlighted that the authors did not use all of the accelerometric data available from AFAD at the time of writing but decided to exempt some stations based on manual scrutiny of the uncorrected time series. In any case, all data used herein are available alongside the supplementary report and/or upon request.

DATA AVAILABILITY STATEMENT
The data that support the findings of this study are available from the corresponding author upon reasonable request.

ORCID
Georgios Baltzopoulos https://orcid.org/0000-0002-0460-6558
Roberto Baraschino https://orcid.org/0000-0002-8363-9306
Eugenio Chioccarelli https://orcid.org/0000-0002-8990-3120
Pasquale Cito https://orcid.org/0000-0001-6603-8106
Iunio Iervolino https://orcid.org/0000-0002-4076-2718

REFERENCES
1. Gülerce Z, Tanvir Shah S, Menekşe A, Arda Özacar A, Kaymakci N, Önder Çetin K. Probabilistic seismic-hazard assessment for east Anatolian fault zone using planar fault source models. *Bull Seismol Soc Am*. 2017;107(5):2353-2366. doi:10.1785/0120170009
2. Danciu L, Nandan S, Reyes C, et al. *The 2020 Update of the European Seismic Hazard Model-ESHM20: Model Overview*. EFEHR Technical Report. 2021. doi:10.12686/a15
3. Zare M, Amini H, Yazdi P, et al. Recent developments of the Middle East catalog. *J Seismol*. 2014;18(4):749-772. doi:10.1007/S10950-014-9444-1/TABLES/9
4. Wald DJ, Quitoriano V, Heaton TH, Kanamori H, Scrivner CW, Worden CB. TriNet "ShakeMaps": rapid generation of peak ground motion and intensity maps for earthquakes in Southern California. *Earthquake Spectra*. 1999;15(3):537-555. doi:10.1193/1.1586057
5. Baltzopoulos G, Baraschino R, Cito P, Chioccarelli E, Iervolino I. Preliminary engineering report on ground motion data of the Feb. 2023 Turkey seismic sequence; 2023. https://www.researchgate.net/publication/368330473_PRELIMINARY_ENGINEERING_REPORT_ON_GROUND_MOTION_DATA_OF_THE_FEB_2023_TURKEY_SEISMIC_SEQUENCE

6. Akkar S, Bommer JJ. Empirical equations for the prediction of PGA, PGV, and spectral accelerations in Europe, the Mediterranean Region, and the Middle East. *Seismol Res Lett*. 2010;81(2):195-206. doi:10.1785/gssrl.81.2.195

7. Gardner JK, Knopoff L. Is the sequence of earthquakes in Southern California, with aftershocks removed, Poissonian? *Bull Seismol Soc Am*. 1974;64(5):1363-1367. doi:10.1785/BSSA0640051363

8. Schmitt R, Herman M, Barnhart W, Furlong K, Benz H. The 2023 Kahramanmaraş, Turkey, Earthquake Sequence. Published March 27, 2023. Accessed April 20, 2023. https://earthquake.usgs.gov/storymap/index-turkey2023.html

9. Stein RS, Toda S, Özbakir AD, et al. Interactions, stress changes, mysteries, and partial forecasts of the 2023 Kahramanmaraş, Türkiye, earthquakes. Published March 2, 2023. Accessed April 20, 2023. https://temblor.net/temblor/insights-stress-changes-mysteries-turkey-earthquakes-2023-15070/

10. Iervolino I, Cito P, Felicetta C, Lanzano G, Vitale A. Exceedance of design actions in epicentral areas: insights from the ShakeMap envelopes for the 2016–2017 central Italy sequence. *Bull Earthquake Eng*. 2021;19(13):5391-5414. doi:10.1007/s10518-021-01192-z

11. Utsu T. A statistical study on the occurrence of aftershocks. *Geophys Mag*. 1961;30:521-605.

12. Reasenberg PA, Jones LM. Earthquake hazard after a mainshock in California. *Science (1979)*. 1989;243(4895):1173-1176. doi:10.1126/SCIENCE.243.4895.1173

13. Kotha SR, Weatherill G, Bindi D, Cotton F. A regionally-adaptable ground-motion model for shallow crustal earthquakes in Europe. *Bull Earthquake Eng*. 2020;18(9):4091-4125. doi:10.1007/s10518-020-00869-1

14. Beyer K, Bommer JJ. Relationships between median values and between aleatory variabilities for different definitions of the horizontal component of motion. *Bull Seismol Soc Am*. 2006;96:1512-1522. doi:10.1785/0120050210

15. Beyer K, Bommer J. Correction - Relationships between median values and between aleatory variabilities for different definitions of the horizontal component of motion. *Bull Seismol Soc Am*. 2007;97(5):1769-1769. doi:10.1785/0120070128

16. Paolucci R, Pacor F, Puglia R, Ameri G, Cauzzi C, Massa M. Record processing in ITACA, the New Italian Strong-Motion Database. In: Akkar S, Gülkan P, van Eck T, eds. *Earthquake Data in Engineering Seismology: Predictive Models, Data Management and Networks*. Springer; 2011:99-113. doi:10.1007/978-94-007-0152-6_8

17. Joyner WB, Boore DM. Peak horizontal acceleration and velocity from strong-motion records including records from the 1979 Imperial Valley, California, earthquake. *Bull Seismol Soc Am*. 1981;71(6):2011-2038. Accessed January 10, 2019. https://pubs.geoscienceworld.org/ssa/bssa/article-abstract/71/6/2011/102109

18. Bommer JJ, Akkar S, Drouet S. Extending ground-motion prediction equations for spectral accelerations to higher response frequencies. *Bull Earthquake Eng*. 2012;10(2):379-399. doi:10.1007/s10518-011-9304-0

19. Anderson JG. Source and site characteristics of earthquakes that have caused exceptional ground accelerations and velocities. *Bull Seismol Soc Am*. 2010;100(1):1-36. doi:10.1785/0120080375

20. Pacor F, Felicetta C, Lanzano G, et al. NESS1: a worldwide collection of strong-motion data to investigate near-source effects. *Seismol Res Lett*. 2018;89(6):2299-2313. doi:10.1785/0220180149

21. Husid RL. Analisis de terremotos: analisis general. *Revista del IDIEM*. 1969;8(1):21-42. https://rchdt.uchile.cl/index.php/RIDIEM/article/view/38536

22. Trifunac MD, Brady AG. A study on the duration of strong earthquake ground motion. *Bull Seismol Soc Am*. 1975;65(3):581-626. doi:10.1785/BSSA0650030581

23. Iervolino I, Chioccarelli E, Baltzopoulos G. Inelastic displacement ratio of near-source pulse-like ground motions. *Earthq Eng Struct Dyn*. 2012;41:2351-2357. doi:10.1002/eqe.2167

24. Baez JI, Miranda E, Amplification factors to estimate inelastic displacement demands for the design of structures in the near field. Proceedings of 12th World Conference on Earthquake Engineering. 2000.

25. Shahi SK, Baker JW. An empirically calibrated framework for including the effects of near-fault directivity in probabilistic seismic hazard analysis. *Bull Seismol Soc Am*. 2011;101(2):742-755. doi:10.1785/0120100090

26. Somerville PG, Smith NF, Graves RW, Abrahamson NA. Modification of empirical strong ground motion attenuation relations to include the amplitude and duration effects of rupture directivity. *Seismol Res Lett*. 1997;68(1):199-222. doi:10.1785/gssrl.68.1.199

27. Burks LS, Baker JW. A predictive model for fling-step in near-fault ground motions based on recordings and simulations. *Soil Dyn Earthquake Eng*. 2016;80:119-126. doi:10.1016/J.SOILDYN.2015.10.010

28. Baker JW. Quantitative classification of near-fault ground motions using wavelet analysis. *Bull Seismol Soc Am*. 2007;97(5):1486-1501. doi:10.1785/0120060255

29. Baltzopoulos G, Luzi L, Iervolino I. Analysis of near-source ground motion from the 2019 Ridgecrest earthquake sequence. *Bull Seismol Soc Am*. 2020;110(4):1495-1505. doi:10.1785/0120200038

30. Iervolino I, Cornell CA. Probability of occurrence of velocity pulses in near-source ground motions. *Bull Seismol Soc Am*. 2008;98(5):2262-2277. doi:10.1785/0120080033